Ultrasonics Sonochemistry 77 (2021) 105672

Contents lists available at ScienceDirect

Ultrasonics Sonochemistry

journal homepage: www.elsevier.com/locate/ultson

Characterization of the structural and dynamic changes of cell wall obtained by ultrasound-water and ultrasound-alkali treatments

Jing Qian, Fengbin Zhao, Jingjing Gao, LiJie Qu, Zhengbin He *, Songlin Yi *

Beijing Key Laboratory of Wood Science and Engineering, College of Material Science and Technology, Beijing Forestry University, No. 35 Tsinghua East Road Haidian District, Beijing, PR China

ARTICLE INFO

Keywords:
Ultrasound
Ultrasound-alkali treatment
Cell wall
Confocal Raman microscopy

ABSTRACT

It is well-known that ultrasound has been studied for its cavitation, mechanical and thermal effects. As a pretreatment technology, ultrasonic alkali treatment has attracted much attention in the field of biomass biochemical transformation. In this study, the structural and dynamic changes of wood cell walls during ultrasound-water, alkali, and ultrasound-alkali treatments were investigated by stereoscopic microscopy, confocal Raman microscopy, Fourier-transform infrared spectroscopy, and X-ray diffraction. The results indicated that the ultrasound-water, alkali, and ultrasound-alkali treatments had the effect of removing extractives from conduits. The uniform self-shrinking samples with shrinkage conduits were obtained by the alkali and ultrasound-alkali treatments. All of the treatments affected the relative content, structure and distribution of the chemical components in the wood cell walls. Compared with water-immersion samples, the relative content of hemicellulose of the treated samples reduced from 32.31% to 7.02% for ultrasound-8% NaOH treated samples. For the signal intensity of lignin, ultrasound-water treated and ultrasound-alkali treated samples displayed a more significant reductions than the alkali treated samples in the cell wall region. The crystal zone and amorphous zone of cellulose coexisted before and after the treatment, for all of the treated samples, and particularly for the ultrasound-assisted treated samples, the crystallinity increased from 38.15% for water-immersion samples to 57.42% for ultrasound-8% NaOH treated samples.

1. Introduction

The modification and conversion of lignocellulosic biomass materials, such as wood, grass, agricultural and forestry residues, has attracted wide interest due to the important role played by lignocellulosic biomass in human society (e.g. in furniture, flooring, and energy) [1–3]. Lignocellulosic biomass is mainly composed of three chemical components (cellulose, hemicellulose and lignin) that are unevenly distributed in the cell wall [4,5]. The distribution, binding mode and properties of the three chemical components in the cell wall have important effects on the macroscopic mechanical properties of the cell wall and the transformation efficiency of lignocellulosic biomass. The cell wall of natural lignocellulosic biomass materials is complex and rigid and is composed of a cellulose microfibril framework tethered together by a coating of hemicellulose and sealed in a waterproof and chemically durable lignin polymeric matrix [6]. As a natural barrier, the fine cell wall in some cases hinders the development of new functional materials such as transparent wood [7], and flame-retardant wood [8], and the achievement of higher energy utilization efficiency (e.g. by enzymatic hydrolysis of biomass [9]). It is important to understand and develop a cost-effective approach for overcoming this recalcitrance.

To date, a series of pretreatments have been applied to different lignocellulosic biomass materials for overcoming the cell wall natural barrier. Lignin is regarded as one of the main factors that leads to the formation of a cell wall barrier [10]. Among these pretreatments, alkali treatment has been widely considered as an efficient method to break the ether and ester bonds in lignin as well as the bonds between lignin and hemicellulose, and thus has the function of disrupting the rigid structure of the cell wall, increasing the porosity and surface area, and swelling the biomass fibers [11]. Furthermore, as an efficient alkaline reagents, sodium hydroxide has been investigated in the field of lignocellulosic biomass processing due to its advantages, such as relatively inexpensive, less energy intensive and high degradation efficiency [12]. The effect of alkali treatment is influenced by many factors, such as temperature, concentration and time [13]. Some studies examined the effect of alkaline treatment parameters on the digestibility of the

* Corresponding authors.
E-mail addresses: hzbcailiao@bjfu.edu.cn (Z. He), ysonglin@126.com (S. Yi).

https://doi.org/10.1016/j.ultsonch.2021.105672
Received 20 March 2021; Received in revised form 1 July 2021; Accepted 12 July 2021
Available online 18 July 2021

substrate to identify whether alkali solution concentration determines the hydrolysis yield [14] and to optimize the process parameters [15–17]. Although numerous studies had reported the information about the influence of alkali treatment on hydrolysis yield and biomass composition [14,49], few references exist on the morphological and histochemical changes of wood cell walls during alkali treatment at room temperature. Understanding the dynamic process of cell wall changes would be important for efficient optimization of the process Therefore, it is valuable to investigate detailed information of spatial and temporal distribution of the main chemical components in cell walls during treatment.

The application of ultrasonic technology in lignocellulosic biomass processing has become a research hotspot [20]. Ultrasonic cavitation is an important parameter in ultrasonic technology that determines the effect of ultrasonic treatment. Ultrasonic cavitation refers to the phenomenon of cavitation bubbles collapse in the liquid caused by the high intensity of an ultrasonic wave with high local energy when the wave passes through liquid medium [21]. This effect enhances mass transfer and heat transfer, improves the activity of the reactant molecules, and increases the probability of their collision with each other. Therefore, ultrasonic treatment had been used as an auxiliary treatment to enhance the effect of other treatments and affect the structure and morphology of woody biomass materials. For example, ultrasonic-assisted extraction can improve the extraction rate, shorten the extraction time and save solvents [22,23]. The ultrasound treatment with different ultrasound power densities induced structural disorganization and changes in the relative crystallinity of the okara fibers [25]. At the same time, ultrasound treatment can destroy wood pits, thus improving wood drying properties to a certain extent, for example by shortening the drying time and improving the drying quality [26].

In recent years, alkali treatment in combination with other novel technologies, such as the ionic liquid treatment [18], and hydrothermal treatment [19], is also being studied extensively, and positive results have been achieved. The combination of alkali treatment with ultrasonic treatment can obtain improved results. Sindhu found that lignin and hemicellulose can be effectively removed by ultrasound-assisted alkali pretreatment [24]. The best hydrolysis performance was obtained after pretreatment by NaOH assisted with ultrasonication and resulted in about 81% of the corresponding theoretical ethanol yield [50]. But, how does ultrasound assist alkali reagent to affect the biochemistry of biomass? It is very important to understand the effect of ultrasound on biomaterial cell wall in order to better combine alkali treatment technology with ultrasonic technology.

Therefore, this work aimed to obtain more information on the cell wall behavior in the ultrasonication environment. The effects of ultrasound-water treatment and ultrasound-alkali treatment on the morphology and chemical compositions of cell wall were investigated. The morphology of oven-dried and moist cell wall, lignin distribution, relative content of chemical components, chemical structure, and crystallinity of Ailanthus altissima were determined. By understanding how wood cell walls respond to ultrasound-alkali treatment, more effective pretreatment strategies can be valuably generated in biomass biochemical transformation.

2. Material and methods

2.1. Materials preparation

A total of 160 Ailanthus altissima (*Ailanthus altissima (Mill.) Swingle in Journ.*) with the dimensions of 20 mm × 20 mm × 20 mm (L × T × R) were sawn from freshly harvested logs. The air dried density and the oven-dried moisture content of the samples were 0.67 ± 0.01 g/cm^3 and 7.89 ± 0.21%, respectively. The samples were provided by Henan Longxiang wood industry (China).

Sodium hydroxide, sodium chlorite, benzene, 95% ethanol, glacial acetic acid, and nitric acid were of analytical grade and were used without further purification. All of the chemicals and distilled water were purchased from Beijing Jialejie Technology Co., Ltd. (China).

2.2. Immersion and ultrasonic treatment

The samples were randomly divided into eight groups and twenty blocks in each group (details were shown in Table 1). The samples underwent the following processing: drying (103 ± 2 °C for 48 h) – weighing – measurement of dimensions – immersion (20 ± 2 °C for 48 h) – ultrasonic treatment (320 W, 25 kHz for 2 h) – neutralization (using distilled water containing 1% acetic acid followed by thoroughly rinsed with distilled water) – drying (103 ± 2 °C for 48 h) – weighing-measurement of dimensions – analysis and characterization. During the ultrasonic treatment process, the temperature of the ultrasonic solution is controlled by a cold water circulation of about 20 °C, as reported in our previous studies [48]. A diagram of the ultrasonic treatment is shown in Fig. 1.

2.3. Physicochemical properties of samples

2.3.1. Stereoscopic microscope

An oven-dried sample of each group was randomly selected, and its cross-section was observed using a stereoscopic microscope (Leica M125, Germany) at a magnification of 50 times and the observed images were recorded.

2.3.2. Confocal Raman microscopy

Prior to Raman analysis, cross-section samples with a thickness of 8 μm were obtained using a sliding microtome. The Raman spectra and images of the 8-μm-thick samples were obtained using a LabRam Xplora confocal Raman microscope (Horiba Jobin-Yvon, Longjumeau, France). The spectrometer is equipped with an Olympus oil microscope (MPlan60×, NA = 1.35) and a 3D motorized platform. The linear-polarized laser (λ = 532 nm) with laser power of 8 mW, scanning interval of 0.6 μm, scanning time of single spectrum of 2 s, pinhole aperture of 300 μm, slit width of 100 μm, and grating of 1200 mm^{-1} was used for scanning.

According to the reports in the literature, Raman spectroscopy can distinguish cell wall layers by identifying different chemical compositions. In addition, average spectra from the regions of interest in the cell wall can be analyzed. The spectra were extracted from the whole image. To eliminate the influence of broad band fluorescence, the obtained Raman spectra were baseline-corrected, and were also smoothed by the Savitsky–Golay algorithm at a moderate level.

2.3.3. Chemical component analysis

All of the samples were oven-dried at 103 ± 2 °C for 24 h prior to being ground into particles. Particles with the mean size of 0.300–0.450 mm were used for chemical component analysis after washing with

Table 1
The experimental design of the study.

Groups	Impregnation condition	Ph	Ultrasonic condition
A_0	distilled water (2d)	8.13 (17.2 °C)	0 h
A_1	distilled water (2d)	8.13 (17.2 °C)	distilled water, 2 h
B_0	1% Sodium hydroxide (2d)	13.24 (16.1 °C)	0 h
B_1	1% Sodium hydroxide (2d)	13.24 (16.1 °C)	1% Sodium hydroxide, 2 h
C_0	4% Sodium hydroxide (2d)	13.67 (16 °C)	0 h
C_1	4% Sodium hydroxide (2d)	13.67 (16.1 °C)	4% Sodium hydroxide, 2 h
D_0	8% Sodium hydroxide (2d)	13.85 (15.5 °C)	0 h
D_1	8% Sodium hydroxide (2d)	13.85 (15.5 °C)	8% Sodium hydroxide, 2 h

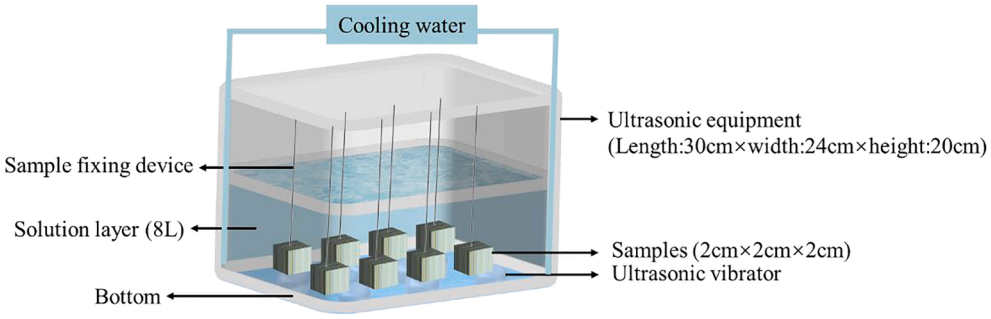

Fig. 1. Diagram of ultrasonic treatment.

distilled water. All of the compound contents were calculated on a dry weight basis. The relative contents of holocellulose and cellulose were measured using the sodium chlorite method (GB/T2677.10-1995, China) and the nitric acid ethanol method (China), respectively [28]. The samples were extracted with benzene-ethanol (2:1 v/v) for 6 h before chemical composition analysis. As for the determination of holocellulose relative content, 2 g extracted wood powder was added into a 250 mL conical flask with 65 mL distilled water, 0.5 mL glacial acetic acid and 0.6 g sodium chlorite. The conical flask was placed in a constant temperature water bath at 75 °C for one hour, and then 0.5 mL glacial acetic acid and 0.6 g of sodium chlorite were continued to be added until the sample turned white. The relative contents of holocellulose and cellulose were obtained by dividing the weight of holocellulose and cellulose by the weight of the extracted sample. The relative contents of hemicellulose and lignin were calculated as the holocellulose relative content minus the cellulose relative content and the total content (100%) minus the holocellulose relative content, respectively. Each determination was repeated six times and the experimental results are averaged over the three nearest data.

2.3.4. Fourier-transform infrared spectroscopy

The samples were milled, and powders with the particle sizes of approximately 75–150 μm were collected and oven-dried prior to characterization. The Fourier-transform infrared (FTIR) spectra of the samples were obtained by infrared spectroscopy (Perkin-Elmer Spectrum GX, USA). Wood powder of each group (10 mg) was used for the measurements. The spectra were obtained in the range of 4000–500 cm^{-1} at a resolution of 4 cm^{-1}.

2.3.5. X-ray diffraction analysis

The powder with a mean particle size of 300–450 um was used for X-ray diffraction (XRD) analysis using a diffractometer (Bruker D8 Advance, Germany) to investigate the changes in crystallinity. Filtered monochromatic radiation with a wavelength of 0.154 nm was generated at a voltage of 40 kV and a current of 40 mA. The samples were scanned at room temperature in the 2θ range of 5–40° with a step size of 0.02° every 0.5 s. The crystallinity of the samples (CrI) was calculated using the Segal method according to:

$$C_rI = \frac{(I_{200} - I_{am})}{I_{200}} \times 100\% \quad (2)$$

where I_{200} is the maximum intensity of the (200) lattice plane diffraction angle, and I_{am} is the scattering intensity of the amorphous background diffraction at the 2θ angle of approximately 18°.

3. Results and discussion

3.1. Stereoscopic microscope observation

The extractives distribution inside the conduit and the morphology of the conduit can be observed from the 50× magnified images in Fig. 2. For the A_0 sample (Fig. 2), crystal gum could be clearly observed in the conduit of the blister 6 h control sample. Ultrasound and alkali treatment effectively removed the crystal gum in the conduit. For the A_0 sample, the shapes of the conduit cells were oval, ellipse and circle and the morphology of the A_1 sample conduits did not change significantly. By contrast, the conduits of the alkali-treated samples (B_0, C_0 and D_0) showed different degrees of shrinkage, the distance between the wood rays became shorter, and the conduit was flattened in the direction of the wood rays. Moreover, with the increase in alkali concentration, the morphological changes became more pronounced. The conduit shapes of the ultrasonication- and alkali-treated samples (shown in B_1, C_1 and D_1) changed more than those of the sample treated with the same alkali concentration. The shape of the conduit of the ultrasound- and 4%

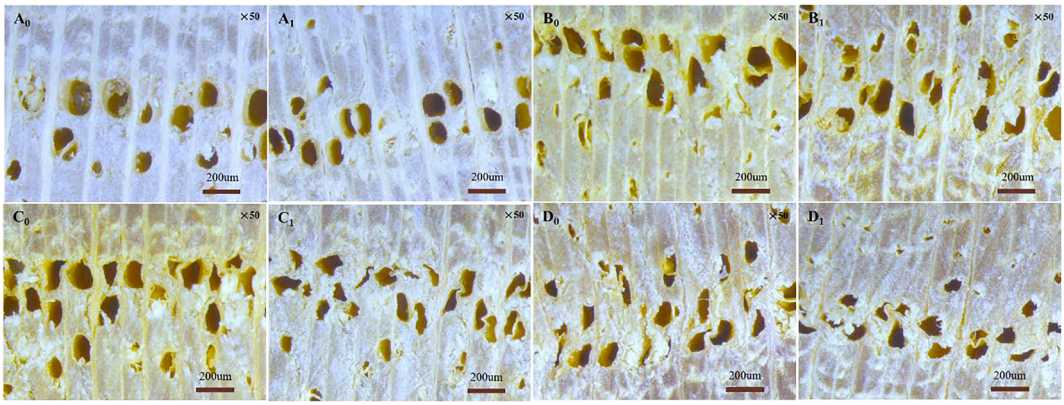

Fig. 2. Cross section of samples under stereoscopic microscope. (A_0) 6 h water-immersion sample, (A_1) 6 h ultrasound-water treated sample, (B_0) 2d 1% sodium hydroxide treated sample, (B_1) 2 h ultrasound-1% sodium hydroxide treated sample, (C_0) 2d 4% sodium hydroxide treated sample, (C_1) ultrasound-4% sodium hydroxide treated sample (D_0) 8% sodium hydroxide treated sample (D_1) ultrasound-8% sodium hydroxide treated sample.

alkali-treated sample was close to that of the 8% alkali treated sample. This may be because the effect of ultrasonic water treatment on the wood cell wall matrix was not as great as that of the alkali treatment. For the A_1 samples, the cell composition of wood did not change drastically (see Table 2). However, the alkali treatment affected the contents of hemicellulose and lignin (see Table 2), so that the wood cell wall layer becomes loose, and shrank after drying. This led to the distance between the adjacent wood rays on the ray parenchyma becoming shorter, which in turn affected the shape of the conduit.

3.2. Confocal raman microscopy analysis

Fig. 3 shows the bright-field images of the samples. As observed from the figure, the cell morphology hardly changed when the cells were moist. Generally, the plant cell wall is composed of the middle lamella (ML), primary cell wall (P), and secondary cell wall (S). Since it is difficult to distinguish the P layer and the ML layer, the P layer and the ML layer are collectively referred to as the compound middle lamella (CML). The common area between three or four cells is called the cell corner middle lamella (CCML) [30]. The chemical composition distributions in the different plant cell wall layers vary, and this can be visualized nondestructively by confocal Raman microscopy. The distribution and intensity of lignin in each layer of the cell wall can be imaged by the integration of the characteristic Raman bands [31,32].

Fig. 4 shows the average Raman spectra in the range of 600–3000 cm^{-1} obtained from the yellow rectangular region of Fig. 3. It is observed from the figure that there was no significant variation in the position of peaks. The main characteristic peaks of cellulose in the figure are 1097, 1454 and 2893 cm^{-1}. Here, 1097 cm^{-1} is the asymmetric stretching vibration peak of the C–O–C glycosidic bond, 1454 cm^{-1} is the stretching vibration of H–C–H and H–O–C, and 2893 cm^{-1} is the stretching vibration of C–H and CH_2. The main characteristic peaks of lignin were 1600 and 1658 cm^{-1}. The Raman shift at 1658 cm^{-1} is attributed to the structure of coniferaldehyde and coniferyl alcohol units, and the Raman shift at 1600 cm^{-1} is attributed to the symmetric stretching vibration of lignin and the benzene ring [33].

The selected region (yellow rectangle in Fig. 3) was used for Raman imaging with the results shown in Fig. 5. Here, the lignin images were acquired by integrating over the characteristic Raman bands in the range of 1547–1707 cm^{-1}. The distributions of lignin in the cell wall of the samples before and after the treatments corresponds to the A_0-D_1 images.

As shown in the A_0 image (Fig. 4), the concentration of lignin was highest in the CCML layer for the untreated sample (black and white areas indicate low and high concentrations of lignin, respectively), followed by the CML layer, and lignin concentration was lowest in the S layer. Even at the same height of the same tree, the distribution and content of the cell wall component vary. Ignoring these subtle and inevitable differences, the lignin distribution of the ultrasound-water sample was similar to that of the untreated sample. However, the intensity of the lignin signal was significantly reduced in A_1. According to the study by Wang et al., the intensity of lignin signal essentially disappeared in the eucalyptus samples hydrothermally treated at 210 °C for 30 min, indicating that a large amount of lignin had been removed from the cell wall [19]. The difference in the lignin signal intensity in ultrasound-water treated samples may be due to the local high temperature and high pressure generated by ultrasound during the ultrasonication pretreatment, resulting in the removal of lignin from the cell wall layer.

For the alkali-immersion samples (shown in B_0, C_0, D_0 of Fig. 5), the distribution pattern of lignin was similar to that of the untreated sample (shown in A_0 of Fig. 5), showing overall a small reduction in the lignin content in the sample. The decrease of lignin in the alkali-immersion samples occurred mainly in the S layer, and the loss of lignin signal intensity in the corner area increased with increasing sodium hydroxide concentration. This observation may be explained as due to the pretreatment solution first penetrating into the S from the cell lumen, thereby leading to the preferential removal of lignin from the S layer [34]. Alternatively, this may be due to the variation in the activity of the lignin units. S-type lignin with a small degree of branching mainly exists in the S layer, and the structure of lignin in the S layer is relatively loose. The CCML region is rich in the G-type lignin, and the structure of G-type lignin is relatively stable, so that the lignin was removed first from the S layer [35,36].

The changes in the lignin distribution are also shown in Fig. 5 (B_1, C_1, D_1). The signal intensity of lignin after ultrasound-assisted alkali treatments was lower than that of the only alkali-treated samples, indicating that ultrasonication can led to the further dissolution of lignin from cell walls. This may be due to the cavitation effect of ultrasonication [37] that enhances the alkali treatment effect in a short time.

Table 2
Chemical composition of samples.

Groups	Cellulose content (%)	Hemicellulose content (%)	Lignin content (%)
A_0	47.49 ± 0.04	32.31 ± 0.04	20.20 ± 0.11
A_1	50.54 ± 0.04	26.88 ± 0.05	21.51 ± 0.10
B_0	46.21 ± 0.04	23.77 ± 0.03	30.02 ± 0.02
B_1	51.65 ± 0.06	15.42 ± 0.04	32.93 ± 0.04
C_0	55.21 ± 0.09	13.58 ± 0.04	31.21 ± 0.05
C_1	57.92 ± 0.07	12.26 ± 0.05	29.82 ± 0.03
D_0	60.35 ± 0.06	9.32 ± 0.03	30.33 ± 0.03
D_1	59.86 ± 0.02	7.02 ± 0.02	33.12 ± 0.02

(A_0) 6 h water-immersion sample, (A_1) 6 h ultrasound-water treated sample, (B_0) 2d 1% sodium hydroxide treated sample, (B_1) 2 h ultrasound-1% sodium hydroxide treated sample, (C_0) 2d 4% sodium hydroxide treated sample, (C_1) ultrasound-4% sodium hydroxide treated sample (D_0) 8% sodium hydroxide treated sample (D_1) ultrasound-8% sodium hydroxide treated sample

3.3. Chemical component analysis

The chemical compositions of water-immersion samples (A_0) and of the samples subjected to alkali treatment (B_0, C_0, D_0) and ultrasonication-assisted pretreatments (A_1, B_1, C_1, D_1) are presented in Table 2. As shown in Table 2, A0 contains 47.49% cellulose, 32.31% hemicellulose and 20.20% lignin. The cellulose and lignin contents of A_1 increased to 50.54% and 21.51%, respectively, after ultrasonic treatment, while the hemicellulose content decreased to 26.88%. The relative content of hemicellulose was strongly affected by the ultrasonic water treatment, which is consistent with our previous study [27]. A dramatic loss of hemicellulose content was observed after the alkali treatment, with lower the hemicellulose content (23.77–9.32%) obtained for higher sodium hydroxide concentrations (1–8%). An ultrasonication-assisted alkali treatment carried out for 2 h showed enhanced effect relative to that of alkali treatment only, and in particular, when 1% sodium hydroxide was used, the relative content of hemicellulose decreased from 23.77% to 15.42%.

Due to the effect of the pretreatment on the hemicellulose content, the relative contents of cellulose and lignin also changed dynamically. Generally, the contents of both were larger than that of A_0 after pretreatment. The lignin content ranged from the initial value of 20.20% to approximately 30% under pretreatments using 1% sodium hydroxide or higher. Combined with the results of the confocal Raman microscopy (see 3.2 for more details), these results show that alkali treatment, water ultrasonic treatment and alkali ultrasonic treatment affected the lignin strength in the cell wall of the wood.

3.4. Fourier-transform infrared spectroscopy

The FTIR spectra and the assignments of their major absorption bands in the range from 4000 to 500 cm^{-1} for the samples obtained with different treatment are shown in Fig. 6 and Table 3. The spectrum of the

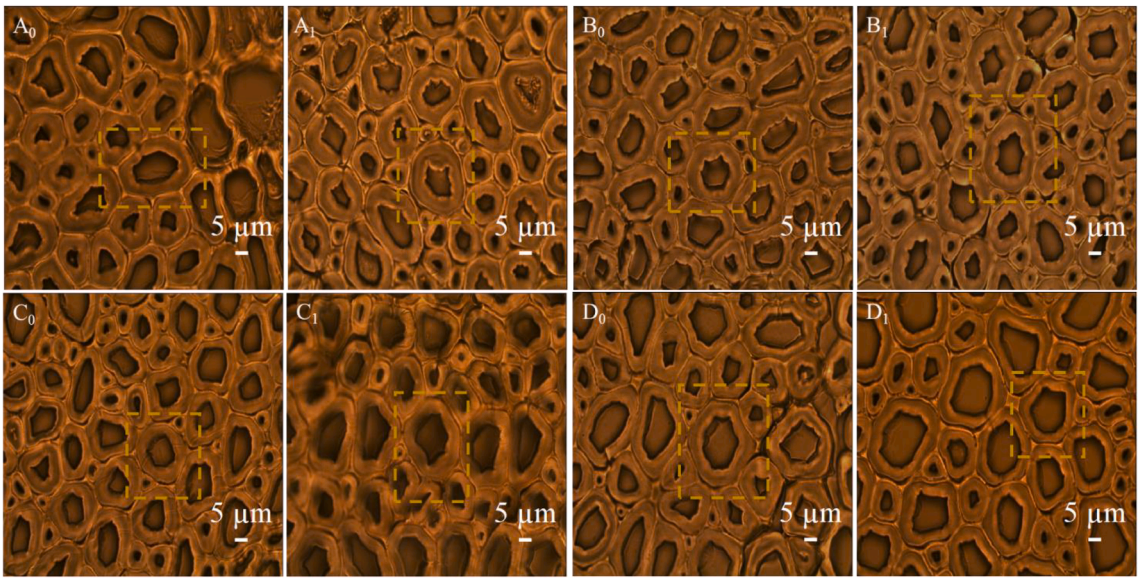

Fig. 3. Bright field images of the cell wall of the samples. Selected areas (yellow rectangle) shown in bright field images were used for Raman imaging. (A_0) 6 h water-immersion sample, (A_1) 6 h ultrasound-water treated sample, (B_0) 2d 1% sodium hydroxide treated sample, (B_1) 2 h ultrasound-1% sodium hydroxide treated sample, (C_0) 2d 4% sodium hydroxide treated sample, (C_1) ultrasound-4% sodium hydroxide treated sample (D_0) 8% sodium hydroxide treated sample (D_1) ultrasound-8% sodium hydroxide treated sample. (For interpretation of the references to colour in this figure legend, the reader is referred to the web version of this article.)

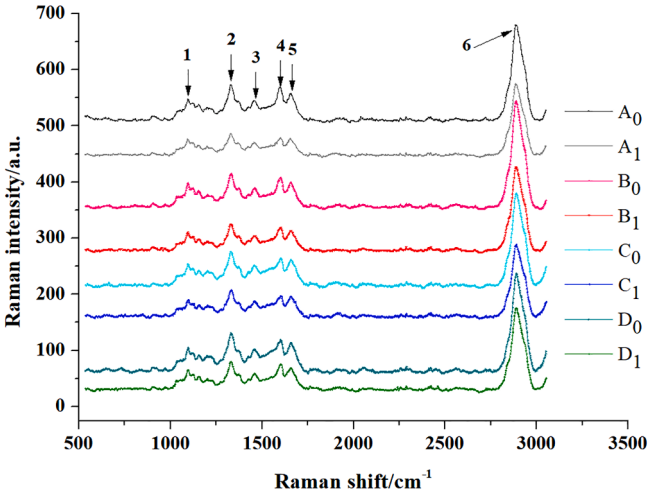

Fig.4. Raman spectrum of samples (A_0) 6 h water-immersion sample, (A_1) 6 h ultrasound-water treated sample, (B_0) 2d 1% sodium hydroxide treated sample, (B_1) 2 h ultrasound-1% sodium hydroxide treated sample, (C_0) 2d 4% sodium hydroxide treated sample, (C_1) ultrasound-4% sodium hydroxide treated sample (D_0) 8% sodium hydroxide treated sample (D_1) ultrasound-8% sodium hydroxide treated sample.

ultrasound-water sample was almost the same as that of the untreated sample. While the spectra of the samples treated by alkali and ultrasound-alkali were found to be different from the spectrum obtained from the untreated sample. A strong hydrogen bonded (O–H) stretching absorption is observed at approximately 3420 cm^{-1} (1) and a prominent C–H stretching absorption is observed at approximately 2900 cm^{-1} [38]. After alkali treatment, the O–H absorption becomes more pronounced, indicating that the hydroxyl group content increases. This may be because the β-aryl ether bond is oxidized and broken to produce new phenolic hydroxyl group, which is consistent with previous research [39].

Only the bands that have been observed to vary from the untreated sample will be discussed here. They are bands at approximately 1742, 1600, 1248 and 1052 cm^{-1}, and are all in the finger-print region between 1800 and 600 cm^{-1}.

For the bands at 1742, 1376, 1158, 1052 and 898 cm^{-1}, the intensities decrease, the band at approximately 1742 cm^{-1} is almost absent and two bands appear at approximately 1052 cm^{-1} after alkali treatment. The aforementioned five bands are assigned as follows: 1) 1742 cm^{-1} for free C═O in xylan (hemicellulose), 2) 1376 cm^{-1} for C–H deformation (cellulose and hemicellulose), 3) 1158 cm^{-1} for C–O–C vibration (cellulose and hemicellulose), 4) 1052 cm^{-1} for C–O stretch (cellulose and hemicellulose), and 5) 898 cm^{-1} for C–H deformation (cellulose) [40,41]. The band at 1742 cm^{-1} can been found in the spectra of the untreated sample (a), however, this band disappeared in the treated samples (B_0, B_1, C_0, C_1, D_0, D_1). Based on the results of Oven's FTIR spectroscopy study of softwood and hardwood in 1989, the FTIR spectra of holocellulose shows a stronger absorption than the lignin component at the band of 1742 cm^{-1} and the absorption of 1742 cm^{-1} is almost certainly related to the stretching of the free carbonyl groups. The polymer composition of wood has a high abundance of free carbonyl groups [42]. Together with the fact that the majority of such carbonyl groups are found in the branched chain hemicellulose polymer, the disappearance of the 1742 cm^{-1} band of the treated samples indicate the removal of hemicellulose by the sodium hydroxide alkali treatment that leads to the disappearance of the free carbonyl groups. The disappearance of the 1742 cm^{-1} band of the alkali treated samples is consistent with Xu's research [29].

In the region near 1600 cm^{-1}, two bands (at approximately 1640 and 1598 cm^{-1}) overlap to form an unusual peak. The 1640 cm^{-1} band is assigned to adsorbed O–H and conjugated C–O, and the 1598–1640 cm^{-1} band is caused by vibrations of the lignin matrix that are most likely associated with the aromatic ring [43]. Moreover, the bands at approximately 1507, 1461, 1427, 1332 and 1112 cm^{-1} are assigned to the aromatic ring in lignin and the absorbed water, C–H asymmetric deformation, C–H deformation in lignin, C–H vibration in cellulose and C–O vibration in syringyl derivatives, and the C–O–C stretching/C–H stretching in the aromatic ring (syringylic), respectively. After alkali treatment, the strength of the 1650 cm^{-1} band is reduced compared to that of the band at 1598 cm^{-1}. According to the study by Mitchell et al. [44], the band at 1650 cm^{-1} can only be removed by drying in situ, and

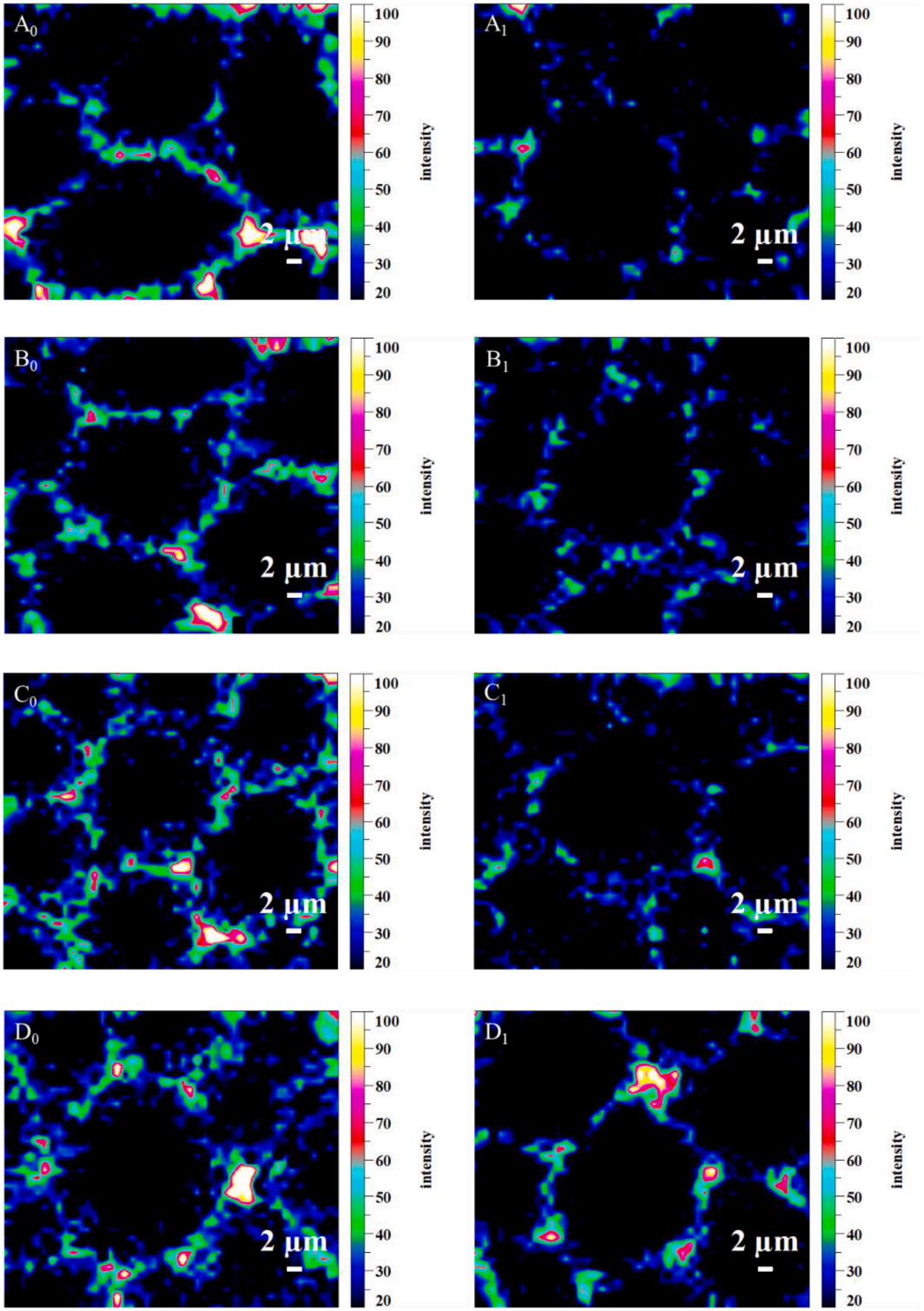

Fig. 5. Raman images of the lignin distribution by integrating from 1547 to 1707 cm^{-1}. (A_0) 6 h water-immersion sample, (A_1) 6 h ultrasound-water treated sample, (B_0) 2d 1% sodium hydroxide treated sample, (B_1) 2 h ultrasound-1% sodium hydroxide treated sample, (C_0) 2d 4% sodium hydroxide treated sample, (C_1) ultrasound-4% sodium hydroxide treated sample (D_0) 8% sodium hydroxide treated sample (D_1) ultrasound-8% sodium hydroxide treated sample.

it appears to be related to the ability of wood to adsorb water.

Differences were also observed between untreated and treated Ailanthus altissima in the region of 1225–1275 cm^{-1}. Only one band is observed at 1248 cm^{-1} in the spectra of untreated Ailanthus altissima, while the 1248 cm^{-1} band disappeared and other two bands at approximately 1228 and 1268 cm^{-1} are shown in the spectra of the treated samples. Previous studies [44,45] have reported that the band at 1248 cm^{-1} appears to arise from the C–O stretching vibration of acetyl and carboxyl groups in the substituted xylans but the lignins contribute absorption bands at 1268 and 1228 cm^{-1} that overlap this band. In the spectra of the untreated sample, the band at 1248 cm^{-1} represents the syringyl ring and C–O stretch in lignin and xylan to some degree [43]. The disappearance of the 1248 cm^{-1} band is likely due to the degradation of the hemicellulose in the sample by the alkali and/or ultrasonic

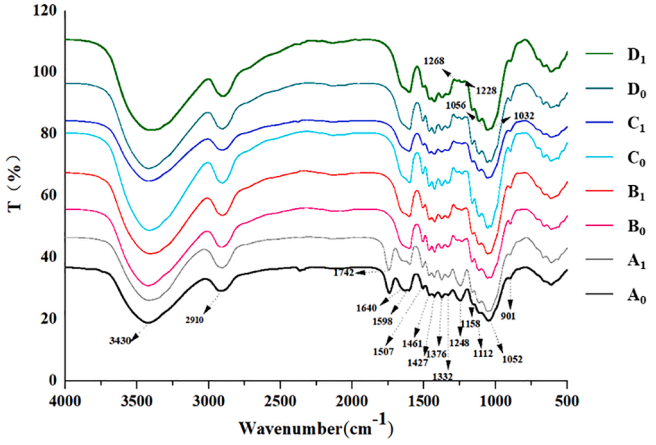

Fig. 6. FTIR spectra of samples. (A_0) 6 h water-immersion sample, (A_1) 6 h ultrasound-water treated sample, (B_0) 2d 1% sodium hydroxide treated sample, (B_1) 2 h ultrasound-1% sodium hydroxide treated sample, (C_0) 2d 4% sodium hydroxide treated sample, (C_1) ultrasound-4% sodium hydroxide treated sample (D_0) 8% sodium hydroxide treated sample (D_1) ultrasound-8% sodium hydroxide treated sample.

treatment. Additionally, the intensity for the bands at approximately 1268 cm^{-1} is almost identical to that at approximately 1228 cm^{-1} in the alkali samples (group B_0, C_0, D_0). However, for the ultrasound-alkali treated samples (groups B_1, C_1, D_1), the intensity of two bands is somewhat weaker than that in the alkali samples, and the lower frequency band at 1228 cm^{-1} is more intense than that at approximately 1268 cm^{-1}. The band at 1268 cm^{-1} is attributed to the combination of the guaiacyl ring vibration, C–O stretching in lignin and C–O linkage in guiacyl aromatic methoxyl groups [46].

3.5. X-ray diffraction analysis

Fig. 7 depicts the X-ray diffraction patterns of the samples. All of the samples showed a 0 0 2 crystal plane peak at approximately 22° and a 101 crystal plane peak between 14.7°and 16.2°. With the application of ultrasound and alkali treatments, the XRD pattern remain intact while the crystallinity (CrI) of the treated samples changed. This indicates that the crystal zone and amorphous zone coexist before and after the treatment.

The CrI of the untreated samples obtained by the peak fitting method was 38.15%, and the CrI of the wood after the ultrasonic water treatment improved to 40.43%, in agreement with previous studies [27]. After alkali treatment at room temperature, the CrI of wood increased, and with the increase in alkali concentration, the crystallinity of wood gradually increased. A CrI of 52% was obtained for the sodium hydroxide concentration of 8%. This may be due to the removal of lignin and partial removal of hemicellulose from the raw materials, and the destruction of amorphous zone of cellulose by swelling of the alkali solution, resulting in an increase in the proportion of the crystallization zone. These results are consistent with the results of previous studies [47], and are supported both by chemical composition analysis (3.3) and Raman laser confocal analysis (3.2). In addition, the CrI of the samples treated by ultrasonication and alkali solution is higher than that of the samples treated by alkali solution only, proving that ultrasonication can promote the alkali treatment effect.

4. Conclusion

Ultrasound-water, alkali, and ultrasound-alkali treatments removed extractives from conduits. The effects of ultrasound-water, alkali, and ultrasound-alkali treatments on the cell wall were as follows. The ultrasound-water treatment decreased the relative hemicellulose content (from 32.31% for the untreated sample to 26.88% for the ultrasound-water treated sample), reduced the signal strength of lignin, and increased the crystallinity of cellulose (from 38.15% for the untreated sample to 40.43% for the ultrasound-water sample). The alkali treatment significantly reduced the hemicellulose relative content, and with the increase in alkali concentration (from 1% to 8%), the hemicellulose relative content decreased (from 23.77% to 9.32%). The alkali treatment increased the crystallinity of cellulose, and the crystallinity gradually increased (41.16% to 52%) with increasing alkali concentration (from 1% to 8%). However, the alkali treatment had little effect on the signal strength of lignin in the cell wall. The ultrasound-alkali treatment further reduced the relative content of hemicellulose and increased the crystallinity of cellulose compared to the alkali treatment. Importantly, the ultrasound-alkali treatment significantly reduced the

Table 3
Assignments of bands in the FTIR spectra of samples.

Wave no. (cm^{-1})									Assignments	Reference
	A_0	A_1	B_0	B_1	C_0	C_1	D_0	D_1		
3420	+	+	+	+	+	+	+	+	O–H stretching (intramolecular hydrogen bonds for cellulose I)	[38–46]
2910	+	+	+	+	+	+	+	+	asymmetrical C–H vibration bands stretching in the methylene group of the polysaccharide compounds	
1742	+	+	–	–	–	–	–	–	free C═O in xylan (hemicellulose)	
1640	+	+	+	+	+	+	+	+	absorbed O–H and conjugated C–O	
1598	+	+	+	+	+	+	+	+	aromatic ring in lignin	
1507	+	+	+	+	+	+	+	+	aromatic ring in lignin and absorbed water	
1461	+	+	+	+	+	+	+	+	C–H asymmetric deformation	
1427	+	+	+	+	+	+	+	+	C–H deformation in lignin	
1376	+	+	+	+	+	+	+	+	C–H deformation in cellulose and hemicellulose	
1332	+	+	+	+	+	+	+	+	C–H vibration in cellulose and C–O vibration in syringyl derivatives	
1268	–	–	+	+	+	+	+	+	Guaiacyl ring breathing, C–O stretching in lignin and C–O linkage in guiacyl aromatic methoxyl groups	
1248	+	+	–	–	–	–	–	–	Syringyl ring and C–O strethching in lignin and xylan	
1228	–	–	+	+	+	+	+	+	C–O and glucopyranosic cycle syringilic sysmmetric vibration	
1158	+	+	+	+	+	+	+	+	C–O–C vibration in cellulose and hemicellulose	
1112	+	+	+	+	+	+	+	+	C–O–C stretching and symmetric vibration of the eater linkage, and C–H stretching in aromatic ring (syringylic)	
1056	–	–	+	+	+	+	+	+	C–O stretching in cellulose and hemicellulose	
1052	+	+	–	–	–	–	–	–		
1032	–	–	+	+	+	+	+	+		
901	+	+	+	+	+	+	+	+	C–H stretching of the cellulose	

(A0) untreated sample, (A1) ultrasonic water untreated sample, (B0) 1% sodium hydroxide treated sample, (B1) ultrasonic 1% sodium hydroxide treated sample, (C0) 4% sodium hydroxide treated sample, (C1) ultrasonic 4% sodium hydroxide treated sample (D0) 8% sodium hydroxide treated sample (D1) ultrasonic 8% sodium hydroxide treated sample.

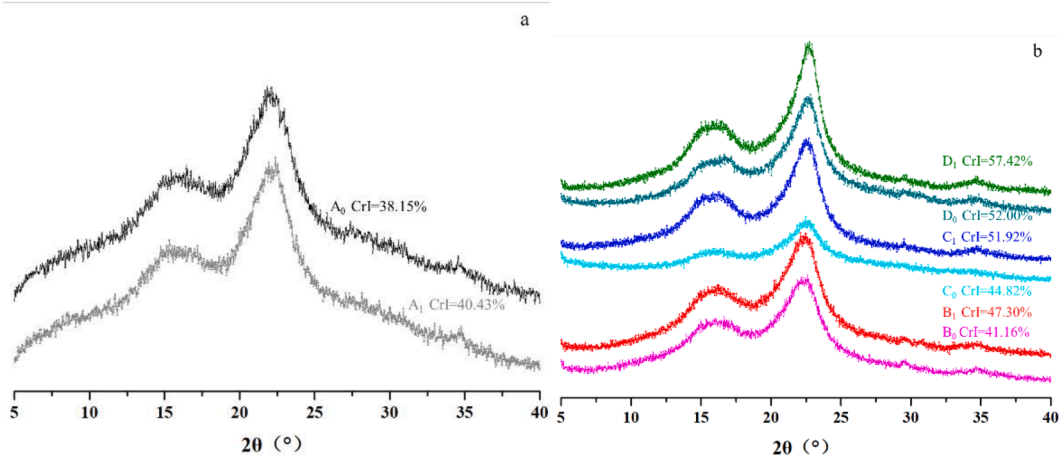

Fig. 7. XRD patterns of samples. (A_0) 6 h water-immersion sample, (A_1) 6 h ultrasound-water treated sample, (B_0) 2d 1% sodium hydroxide treated sample, (B_1) 2 h ultrasound-1% sodium hydroxide treated sample, (C_0) 2d 4% sodium hydroxide treated sample, (C_1) ultrasound-4% sodium hydroxide treated sample (D_0) 8% sodium hydroxide treated sample (D_1) ultrasound-8% sodium hydroxide treated sample.

signal intensity of lignin in the cell wall compared to alkali treatment. In conclusion, ultrasonication is a clean and effective treatment method that has great potential for breaking down cell wall barriers of lignocellulosic biomass materials.

CRediT authorship contribution statement

Jing Qian: Conceptualization, Methodology, Validation, Formal analysis, Investigation, Writing - original draft, Writing - review & editing, Project administration. **Fengbin Zhao:** Investigation. **Jingjing Gao:** Investigation. **LiJie Qu:** Investigation. **Zhengbin He:** Supervision, Funding acquisition. **Songlin Yi:** Resources, Funding acquisition.

Declaration of Competing Interest

The authors declare that they have no known competing financial interests or personal relationships that could have appeared to influence the work reported in this paper.

Acknowledgements

We gratefully acknowledge the financial support of the National Science Foundation of China: the Mechanism of Ultrasound Promotion Heat and Mass Transfer within Boundary Layer during Wood Drying (31600457) and the Special Research Project of Forestry Public Welfare Industry: Study and demonstration on key technology of wood furniture manufacturing in low quality plantation (201404502).

References

[1] Y.M. Dong, S.F. Zhang, J.Z. Li, Research progress in wood cell wall modification, J. For. Eng. 2 (2017) 34–39, https://doi.org/10.13360/j.issn.2096-1359.2017.04.006.
[2] G.J. Vargas Betancur, N. Pereira, Sugar cane bagasse as feedstock for second generation ethanol production. Part I: Diluted acid pretreatment optimization, Electron. J. Biotechnol. 13 (2010) 1–9, https://doi.org/10.2225/vol13-issue3-fulltext-3.
[3] Y. Uju, A. Shoda, M. Nakamoto, W. Goto, Y. Tokuhara, S. Noritake, N. Katahira, K. Ishida, C. Nakashima, Ogino, Short time ionic liquids pretreatment on lignocellulosic biomass to enhance enzymatic saccharification, Bioresour. Technol. 103 (2012) 446–452, https://doi.org/10.1016/j.biortech.2011.10.003.
[4] L. Sun, B.A. Simmons, S. Singh, Understanding tissue specific compositions of bioenergy feedstocks through hyperspectral Raman imaging, Biotechnol. Bioeng. 108 (2011) 286–295, https://doi.org/10.1002/bit.22931.
[5] M. Williams, G. Freshour, A.G. Darvill, P. Albersheim, M.G. Hahn, An antibody fab selected from a recombinant phage display library detects deesterified pectic polysaccharide rhamnogalacturonan II in plant cells, Plant Cell 8 (1996) 673–685, https://doi.org/10.2307/3870343.
[6] M.E. Himmel, S.-Y. Ding, D.K. Johnson, W.S. Adney, M.R. Nimlos, J.W. Brady, T. D. Foust, Biomass recalcitrance: engineering plants and enzymes for biofuels production, Science 315 (5813) (2007) 804–807, https://doi.org/10.1126/science.1137016.
[7] Y. Wu, C.Y. Tang, J.M. Wu, Q.T. Huang, Research progress of transparent wood: a review, J. For. Eng. 3 (2018) 12–18, https://doi.org/10.13360/j.issn.2096-1359.2018.04.002.
[8] M.Z. Pan, C.X. Ding, S. Zhang, Y.P. Huang, Progress on flame retardancy of wood plastic composites, J. For. Eng. 5 (2020) 1–12, https://doi.org/10.13360/j.issn.2096-1359.202001020.
[9] H. Chen, J. Liu, X. Chang, D. Chen, Y. Xue, P. Liu, H. Lin, S. Han, A review on the pretreatment of lignocellulose for high-value chemicals, Fuel Process. Technol. 160 (2017) 196–206, https://doi.org/10.1016/j.fuproc.2016.12.007.
[10] S.B. Mishra, A.K. Mishra, N.K. Kaushik, M.A. Khan, Study of performance properties of lignin-based polyblends with polyvinyl chloride, J. Mater. Process. Technol. 183 (2-3) (2007) 273–276, https://doi.org/10.1016/j.jmatprotec.2006.10.016.
[11] J.S. Kim, Y.Y. Lee, T.H. Kim, A review on alkaline pretreatment technology for bioconversion of lignocellulosic biomass, Bioresour. Technol. 119 (2016) 42–48, https://doi.org/10.1016/j.biortech.2015.08.085.
[12] A. Isogai, R.H. Atalla, Dissolution of cellulose in aqueous NaOH solutions, Cellulose 5 (1998) 309–319, https://doi.org/10.1023/A:1009272632367.
[13] H.K. Choi, S.I. Kwon, Multiscale modeling and predictive control of cellulose accessibility in alkaline pretreatment for enhanced glucose yield, Fuel 280 (2020), https://doi.org/10.1016/j.fuel.2020.118546.
[14] Y.e. Chen, M.A. Stevens, Y. Zhu, J. Holmes, H. Xu, Understanding of alkaline pretreatment parameters for corn stover enzymatic saccharification, Biotechnol. Biofuels 6 (1) (2013) 8, https://doi.org/10.1186/1754-6834-6-8.
[15] Y.S. Cheng, Y. Zheng, C.W. Yu, T.M. Dooley, B.M. Jenkins, J.S. Vandergheynst, Evaluation of high solids alkaline pretreatment of rice straw, Appl. Biochem. Biotechnol. 162 (2010) 1768–1784, https://doi.org/10.1007/s12010-010-8958-4.
[16] B.Y. Chen, S.W. Chen, H.T. Wang, Use of different alkaline pretreatments and enzyme models to improve low-cost cellulosic biomass conversion, Biomass Bioenergy 39 (2012) 182–191, https://doi.org/10.1016/j.biombioe.2012.01.012.
[17] S. Mclntosh, T. Vancov, Optimisation of dilute alkaline pretreatment for enzymatic saccharification of wheat straw, Biomass Bioenergy 35 (2011) 3094–3103, https://doi.org/10.1016/j.biombioe.2011.04.018.
[18] H.Y. Li, X. Chen, C.Z. Wang, S.N. Sun, R.C. Sun, Evaluation of the two-step treatment with ionic liquids and alkali for enhancing enzymatic hydrolysis of Eucalyptus: chemical and anatomical changes, Biotechnol. Biofuels 9 (2016) 166, https://doi.org/10.1186/s13068-016-0578-y.
[19] C.Z. Wang, H.Y. Li, M.F. Li, J. Bian, R.C. Sun, Revealing the structure and distribution changes of Eucalyptus lignin during the hydrothermal and alkaline pretreatments, Sci. Rep. 593 (2017) 1–10, https://doi.org/10.1038/s41598-017-00711-w.
[20] L.W. Bi, Z.D. Zhao, M. Vinatoru, Y.P. Chen, D.M. Li, Y. Gu, J. Wang, Research progress of application of ultrasonic technology to biomass resources processing, Chem. Ind. For. Prod. 27 (2007) 138–142, https://doi.org/10.3321/j.issn:0253-2417.2007.z1.033.
[21] F. Chemat, N. Rombaut, A.-G. Sicaire, A. Meullemiestre, A.-S. Fabiano-Tixier, M. Abert-Vian, Ultrasound assisted extraction of food and natural products. Mechanisms, techniques, combinations, protocols and applications a review, Ultrason. Sonochem. 34 (2017) 540–560, https://doi.org/10.1016/j.ultsonch.2016.06.035.
[22] S. Hemwimol, P. Pavasant, A. Shotipruk, Ultrasound-assisted extraction of anthraquinones from roots of Morinda citrifolia, Ultrason. Sonochem. 13 (2006) 543–548, https://doi.org/10.1016/j.ultsonch.2005.09.009.

[23] M. Vinatoru, An overview of the ultrasonically assisted extraction of bioactive principles from herbs, Ultrason. Sonochem. 8 (2001) 303–313, https://doi.org/10.1016/S1350-4177(01)00071-2.
[24] R. Sindhu, P. Binod, A.K. Mathew, A. Abraham, E. Gnansounou, S.B. Ummalyma, L. Thomas, A. Pandey, Development of a novel ultrasound-assisted alkali pretreatment strategy for the production of bioethanol and xylanases from chili post harvest residue, Bioresour. Technol. 242 (2017) 146–151, https://doi.org/10.1016/j.biortech.2017.03.001.
[25] X.J. Fan, H.D. Chang, Y.A. Lin, X.M. Zhao, A. Zhang, S. Li, Z. Feng, X. Chen, Effects of ultrasound-assisted enzyme hydrolysis on the microstructure and physicochemical properties of okara fibers, Ultrason. Sonochem. 69 (2020), https://doi.org/10.1016/j.ultsonch.2020.105247.
[26] S. Qiu, Z.Y. Wang, Z.B. He, S.L. Yi, Effect of ultrasonic pretreatment on drying characteristic of polar, J. Northeast For. Univ. 44 (2016) 35–38, https://doi.org/10.3969/j.issn.1000-5382.2016.02.009.
[27] J. Qian, Y.J. Li, J.J. Gao, Z.B. He, S.L. Yi, The effect of ultrasonic intensity on physicochemical properties of Chinese Fir, Ultrason. Sonochem. 64 (2020), https://doi.org/10.1016/j.ultsonch.2020.104985.
[28] Q.Z. Chen, H. Zhu, Fibrous raw material – determination of holocellulose: GB/T 2677.10, National Standard of the People's Republic of China, China Standard Press, China, 1995, pp. 220–223.
[29] J. Xu, E.F. Krietemeyer, V.M. Boddu, S.X. Liu, W.-C. Liu, Production and characterization of cellulose nanofibril (CNF) from agricultural waste corn stover, Carbohydr. Polym. 192 (2018) 202–207, https://doi.org/10.1016/j.carbpol.2018.03.017.
[30] Y.H. Zhu, L. Wen, Y.L. Zhang, X.Z. Wang, Visualization of micro-structure and chemical composition of polar tension wood, J. For. Eng. 5 (2020) 54–58.
[31] M. Schmidt, A.M. Schwartzberg, P.N. Perera, A. Weber-Bargioni, A. Carroll, P. Sarkar, E. Bosneaga, J.J. Urban, J. Song, M.Y. Balakshin, E.A. Capanema, M. Auer, P.D. Adams, V.L. Chiang, P.J. Schuck, Perera, Weber-Bargioni, Carroll, Sarkar, Bosneaga, Urban, Label-free in situ imaging of lignification in the cell wall of low lignin transgenic Populus trichocarpa, Planta 230 (3) (2009) 589–597, https://doi.org/10.1007/s00425-009-0963-x.
[32] L.Q. Chu, R. Masyuko, J.V. Sweedler, P.W. Bohn, Base-induced delignification of Miscanthus × giganteus studied by three-dimensional confocal Raman imaging, Bioresour. Technol. 101 (2010) 4919–4925, https://doi.org/10.1016/j.biortech.2009.10.096 (2010).
[33] U.P. Agarwal, D.M. James, A. Sally, FT-Raman investigation of milled-wood lignins: softwood, hardwood, and chemically modified black spruce lignins, J. Wood Chem. Technol. 31 (2011) 324–344, https://doi.org/10.1080/02773813.2011.562338.
[34] Z. Ji, J. Ma, F. Xu, Multi-scale visualization of dynamic changes in poplar cell walls during alkali pretreatment, Microsc. Microanal. 20 (2) (2014) 566–576, https://doi.org/10.1017/S1431927614000063.
[35] L.A. Donaldson, Lignification and lignin topochemistry – an ultrastructural view, Phytochemistry 57 (6) (2001) 859–873, https://doi.org/10.1016/S0031-9422(01)00049-8.
[36] M.H. Studer, J.D. DeMartini, M.F. Davis, R.W. Sykes, B. Davison, M. Keller, G. A. Tuskan, C.E. Wyman, Lignin content in natural Populus variants affects sugar release, Proc. Natl. Acad. Sci. 108 (2011) (2011) 6300–6305, https://doi.org/10.1073/pnas.1009252108.
[37] A.M. Basedow, K.H. Ebert, Ultrasonic degradation of polymers in solution, Adv. Polym. Sci. 22 (1977) 83–148, https://doi.org/10.1007/3-540-07942-4_6.
[38] K.K. Pandey, A study of chemical structure of soft and hardwood and wood polymers by FTIR spectroscopy, J. Appl. Polym. Sci. 71 (12) (1999) 1969–1975, https://doi.org/10.1002/(ISSN)1097-4628.
[39] M.L. Nelson, R.T. O'Connor, Relation of certain infrared bands to cellulose crystallinity and crystal latticed type. Part I. Spectra of lattice types I, II, III and of amorphous cellulose, J. Appl. Polym. Sci. 8 (1964) 1311–1324, https://doi.org/10.1002/app.1964.070080322.
[40] K.J. Harrington, H.G. Higgins, A.J. Michell, Infrared spectra of Eucalypus regnans F. Muell. and Pinus radiata D.Don, Holzforschung 18 (1964) 108–113, https://doi.org/10.1515/hfsg.1964.18.4.108.
[41] T.P. Schultz, W.G. Glasser, Quantitative structural analysis of lignin by diffuse reflectance fourier transform infrared spectrometry, Holzforschung 40 (1986) 37–44.
[42] N.L. Owen, D.W. Thomas, Infrared studies of "hard" and "soft" woods, Appl. Spectrosc. 43 (1989) 451–455, https://doi.org/10.1366/0003702894202760.
[43] K.K. Pandey, A.J. Pitman, FTIR studies of the changes in wood chemistry following decay by brown-rot and white-rot fungi, Int. Biodeterior. Biodegrad. 52 (2003) 151–160, https://doi.org/10.1016/S0964-8305(03)00052-0.
[44] A.J. Michell, H.D. Ingle, C.M. Stewart, Infrared spectra of some woods of taxonomic interest, Wood Sci. Technol. 3 (1969) 93–99, https://doi.org/10.1007/BF00639633.
[45] R.H. Marchessault, Application of infra-red spectroscopy to cellulose and wood polysaccharides, Pure Appl. Chem. 5 (1962) 107–130, https://doi.org/10.1351/pac196205010107.
[46] H. Chen, C. Ferrari, M. Angiuli, J. Yao, C. Raspi, E. Bramanti, Qualitative and quantitative analysis of wood samples by Fourier transform infrared spectroscopy and multivariate analysis, Carbohydr. Polym. 82 (2010) 772–778, https://doi.org/10.1016/j.carbpol.2010.05.052.
[47] J. Zhao, F.R. Zhang, M. Chen, C. Xu, C.S. Quan, S.D. Fan, Effect of NaOH pretreatments on cellulosic structure and enzymatic hydrolysis of corn stover, J. Agro-Environ. Sci. 35 (2016) 1407–1412, https://doi.org/10.11654/jaes.2016.07.025.
[48] Z.Y. Wang, L.J. Qu, J. Qian, Z.B. He, S.L. Yi, Effects of the ultrasound-assisted pretreatments using borax and sodium hydroxide on the physicochemical properties of Chinese fir, Ultrason. Sonochem. 50 (2019) 200–207, https://doi.org/10.1016/j.ultsonch.2018.09.017.
[49] T. Persson, J.L. Ren, E. Joelsson, A.-S. Jönsson, Fractionation of wheat and barley straw to access high-molecular-mass hemicelluloses prior to ethanol production, Bioresour. Technol. 100 (17) (2009) 3906–3913, https://doi.org/10.1016/j.biortech.2009.02.063.
[50] A. Goshadrou, K. Karimi, M.J. Taherzadeh, Bioethanol production from sweet sorghum bagasse by Mucor hiemalis, Ind. Crops Prod. 34 (2011) 1219–1225, https://doi.org/10.1016/j.indcrop.2011.04.018.